Spin effects in double photoionization of lithium

A. S. Kheifets*
Research School of Physics and Engineering, The Australian National University, Canberra, Australian Capital Territory 0200, Australia

D. V. Fursa, C. W. Hines, and I. Bray
Institute of Theoretical Physics, Curtin University, Perth, Western Australia 6845, Australia

J. Colgan
Theoretical Division, Los Alamos National Laboratory, Los Alamos, New Mexico 87545, USA

M. S. Pindzola
Department of Physics, Auburn University, Auburn, Alabama 36849, USA
(Received 9 December 2009; published 22 February 2010)

We apply the nonperturbative convergent close-coupling (CCC) and time-dependent close coupling (TDCC) formalisms to calculate fully differential energy and angular resolved cross sections of double photoionization (DPI) of lithium. The equal energy sharing case is considered in which dynamics of the DPI process can be adequately described by two symmetrized singlet and triplet amplitudes. The angular width of these amplitudes serves as a measure of the strength of the angular correlation between the two ejected electrons. This width is interpreted in terms of the spin of the photoelectron pair.

DOI: 10.1103/PhysRevA.81.023418 PACS number(s): 32.80.Fb, 32.30.Rj, 32.70.−n, 31.15.ve

I. INTRODUCTION

The lithium atom is the simplest many-electron target beyond helium which can be studied by means of single-photon two-electron ionization. Such a double photoionization (DPI) process is driven entirely by many-electron correlations and thus offers a sensitive probe of correlated electronic structure.

Up to now, DPI studies of Li have been limited to the total integrated cross section (TICS), which was determined over a wide range of photon energies. Experimentally, the ratio of double-to-single photoionization cross sections was measured and then normalized to the known single photoionization cross section [1,2]. Theoretically, various nonperturbative computational schemes were applied such as time-dependent close coupling (TDCC), R matrix with pseudostates (RMPS), and convergent close-coupling (CCC) methods. The TDCC calculation above the double K-shell ionization threshold [3] compared favorably with experimental data [4]. Below this threshold, both the TDCC and RMPS theories [5] as well as the CCC theory [6] produced very similar DPI cross sections. However, the peak cross-section value was about 15% higher than the corresponding experimental maximum. This difference can be attributed to normalization of the experimental data to a somewhat lower single photoionization cross section obtained in an older calculation [7].

Apart from numerical values, some qualitative features of DPI of Li can be inferred from experiment and theory. For instance, by scaling the double-to-single photoionization cross-section ratio in Li with that of He, Wehlitz *et al.* [8] were able to demonstrate the dominance of the intermediate triplet state $1s2s\,^3S$ of Li^+ as the precursor of DPI of Li [8]. A similar conclusion was reached in an explicitly spin resolved CCC calculation [6].

More insight into the DPI process can be gained from analyzing the fully differential cross section which is resolved with respect to the photoelectrons escape angles Ω_1, Ω_2 and energies E_1, E_2. This quantity is known as the triply differential cross sections (TDCS), where one of the photoelectron energies can be deduced from the energy conservation $E_1 + E_2 = \omega - I_P^{++}$. Here ω is the photon energy and $I_P^{++} = 81.0\,\text{eV}$ is the first double ionization potential of Li [9]. In the present paper, we perform CCC and TDCC calculations of TDCS of 91-eV photons incident on the ground state of Li and report our data for the case $E_1 = E_2 = 5\,\text{eV}$.

In addition to numerical results, we offer a general parametrization of the TDCS which requires a set of fully symmetric and antisymmetric amplitudes in the singlet and triplet channels (four amplitudes in total). The case of equal energy sharing $E_1 = E_2$ is particularly instructive as only a pair of symmetric amplitudes in the singlet and triplet channel is needed to describe the dynamics of the DPI process. As the kinematic factors in these channels are different, one can selectively turn them on and off by choosing a certain combination of the photoelectron escape angles. Here we consider the coplanar geometry in which both photoelectron momenta $\boldsymbol{k}_1, \boldsymbol{k}_2$ and direction of the polarization vector $\boldsymbol{e}$ belong to the same plane. In this case, the two configurations $\boldsymbol{k}_1 \perp \boldsymbol{e}$ and $\boldsymbol{k}_1 \parallel \boldsymbol{e}$ correspond to the overwhelming dominance of the singlet and triplet channels, respectively, with both channels contributing partially in between.

The dynamics of the DPI process embedded in the singlet and triplet amplitudes favors antiparallel escape in order to minimize the Coulomb repulsion between the two photoelectrons. Correspondingly, both amplitudes peak at the back-to-back emission and the mutual photoelectron angle

*Corresponding author: A.Kheifets@anu.edu.au

$\theta_{12} = 180^\circ$. The width of the amplitudes around this maximum indicates the strength of the angular correlation between the two ejected electrons. This strength turns out to be larger in the singlet channel as compared to the triplet channel. We interpret this phenomenon in terms of the spatial exchange symmetry of the two-electron continuum wave function.

II. FORMALISM

A. CCC method

Application of the CCC method to DPI of Li is described in detail in our earlier publication [6]. In brief, the ionization amplitude is written as the matrix element of the dipole operator between the multiconfiguration initial state $\langle 0, 1, 2|i\rangle$ and the final multichannel state. The latter is expanded over the set of channel states, each of which is a product of the Li^+ ion target state $\langle 0, 1|\alpha\rangle$ and a distorted wave $\langle 2|\boldsymbol{k}\rangle$. The target electrons are labeled 0, 1 and the continuum electron is tagged 2. The label $\alpha \equiv NLS$ comprises the integer N, which numbers the set of target states, with the given orbital momentum L and spin S. The expansion coefficients of the final multichannel state are the corresponding elements of the half-on-shell T matrix, which is found by solving a set of integral Lippmann-Schwinger equations. The negative energy target states $\mathcal{E}_\alpha < 0$ are attributed to single photoionization whereas the positive energy states $\mathcal{E}_\alpha > 0$ contribute to DPI.

The angular and radial variables are separable in the CCC formalism. The T-matrix integrated dipole matrix element, which is stripped of its angular dependence, is written as

$$D_{\alpha l}(k) = d_{\alpha l}(k) + \sum_{\beta l'} \int\!\!\!\!\!\!- \frac{\langle \alpha l k \parallel T \parallel \beta l' k'\rangle \, d_{\beta l'}(k')}{E - k'^2/2 - \mathcal{E}_\beta + i\delta}. \qquad (1)$$

Here k, l denote the linear and angular momenta of the continuous electron state and $E = k^2/2 + \mathcal{E}_\alpha$ is the total energy of the scattering system, which consists of the photoelectron and the Li^+ ion. The bare dipole matrix elements $d_{\alpha l}(k)$ are expressed via radial integrals containing the ground- and final-state orbitals and the dipole operator either in the length $\sum_{j=1}^{3} r_j$ or velocity $\omega^{-1} \sum_{j=1}^{3} \nabla_j$ gauges.

The reduced dipole matrix element Eq. (1) is used to construct the DPI matrix element, which corresponds to ejection of the photoelectron pair with the linear momenta k_1, k_2 and the angular momenta l_1, l_2:

$$D_{S\, l_1 l_2}(k_1, k_2) = (-i)^{l_1+l_2}\, e^{i[\sigma_{l_1}(Z=2)+\sigma_{l_2}(Z=1)]} \times D_{\alpha l_2}(k_2)\, \langle l_1 k_1, 1s \parallel \alpha\rangle. \qquad (2)$$

Here $\langle l_1 k_1, 1s \parallel \alpha\rangle$ is the radial projection of the positive energy target state α of the matching energy $\mathcal{E}_\alpha = k_1^2/2$ to the final ionized state. The latter state is composed of the photoelectron $l_1 k_1$ and the bound electron frozen to the $1s$ state. Such a freezing of the target electron corresponds to restriction of the final double ionized channel to the Li^{2+} ion in its ground state. The two photoelectrons are treated on a different footing. The slow or "inner" photoelectron $l_1 k_1$ is moving in the field of the double charged ion whereas the faster "outer" photoelectron $l_2 k_2$ experiences the nuclear charge screened by the inner photoelectron. This explains the expressions for the Coulomb phases σ_l in Eq. (2).

This notion of inner and outer electrons makes sense only when $E_1 < E_2$. The equal energy sharing case $E_1 = E_2$ requires special treatment. The spin S in Eq. (2) is related to the positive energy target state $\langle 0, 1|\alpha\rangle$, with $\alpha \equiv NLS$ but not the photoelectron pair 1, 2. Indeed, the spin part of the final-state wave function has the form [10]

$$\chi_{SSM}(0, 1, 2) = \sum_{M\,\mu} C^{SM}_{SM,\frac{1}{2}\mu}\, \chi_{SM}(0, 1)\chi_{\frac{1}{2}\mu}(2), \qquad (3)$$

where the total spin of the collision system is $\mathcal{S} = 1/2$. Following the development of equal energy sharing e-He ionization [10], the spins can be recoupled to an alternative state

$$\chi_{SSM}(1, 2, 0) = \sum_{S'=0,1} \chi_{S'SM}(0, 1, 2)\, \gamma_{SS'}, \qquad (4)$$

which corresponds to the total spin S of the photoelectron pair. The recoupling coefficients $\gamma_{SS'}$ are expressed via $6j$ symbols. The spin transformation (4) leads to an alternative set of DPI matrix elements,

$$\tilde{D}_{S\, l_1 l_2}(k_1, k_2) = \sum_{S'=0,1} [(-1)^{S'} D_{S'\, l_1 l_2}(k_1, k_2) + D_{S'\, l_2 l_1}(k_1, k_2)\gamma_{SS'}], \qquad (5)$$

which possesses an explicit exchange symmetry

$$\tilde{D}_{S\, l_1 l_2}(k_1, k_2) = (-1)^S\, \tilde{D}_{S\, l_2 l_1}(k_1, k_2) \qquad (6)$$

as the index S now refers to the spin of the photoelectron pair.

The matrix elements (2) for $E_1 < E_2$ or the alternative set (5) for $E_1 = E_2$,

$$F_{S\, l_1 l_2}(k_1, k_2) = \begin{cases} D_{S\, l_1 l_2}(k_1, k_2), & k_1 \neq k_2, \\ \tilde{D}_{S\, l_1 l_2}(k_1, k_2), & k_1 = k_2, \end{cases} \qquad (7)$$

are then fed to the following expression for the TDCS, which takes the form of the partial wave expansion:

$$\frac{d^3\sigma}{d\Omega_1 d\Omega_2\, dE_2} = C \sum_{S=0,1} \left| \sum_{l_1 l_2} \boldsymbol{e} \cdot \mathcal{Y}_1^{l_1 l_2}(\boldsymbol{n}_1, \boldsymbol{n}_2)\, F_{S\, l_1 l_2}(k_1, k_2) \right|^2, \qquad (8)$$

where $C = 8\pi^2\omega/(3c)$ is the photoionization constant and $c \simeq 137$ is the speed of light in atomic units. The unit vectors $\boldsymbol{n}_i = \boldsymbol{k}_i/k_i$, $i = 1, 2$, are directed along the photoelectron momenta. The bipolar harmonics are tensors of rank 1 expressed by the following tensorial product [11]:

$$\mathcal{Y}_1^{l_1 l_2}(\boldsymbol{n}_1, \boldsymbol{n}_2) = Y_{l_1}(\boldsymbol{n}_1) \otimes Y_{l_2}(\boldsymbol{n}_2). \qquad (9)$$

The computational implementation has required considerable extension of the present CCC code. The calculations involve the calculation of the T- and d-matrix elements in Eq. (2). The former arise upon solution of electron scattering on the He-like Li^+. The CCC formalism for doing so has been given in [12]. Convergence needs to be established as a function of the Laguerre basis parameters λ_l and N_l for $l \leqslant l_{\max}$. As was done previously, to reduce the number of free parameters we set $\lambda_l = \lambda$ and $N_l = N_0 - l$, leaving only three parameters to choose: λ, N_0, and $l_{\max}$. Presently, we took

$\lambda = 2$, $N_0 = 40$, and $l_{\max} = 7$. With these choices we have a good coverage of the Li^+ discrete (and open, below 10 eV) continuum. The resulting equations to be solved required solutions of a set of linear equations with matrices in excess of 80,000 by 80,000. For efficient numerical implementation we have created a hybrid OPENMP-MPI implementation of the code that uses SCALAPACK for solving the linear equations. Using 24 cores the calculations take around 30 minutes.

B. TDCC method

A description of the TDCC approach to DPI of Li was recently presented [5]. In the two-electron formulation, two calculations are made, one for the two photoelectrons coupling to a singlet state and one for both photoelectrons coupling to a triplet state. After propagation of the Schrödinger equation, one can obtain the final momentum-space amplitudes using

$$P^{LS}_{l_1 l_2}(k_1, k_2, T) = \int_0^\infty dr_1 \int_0^\infty dr_2 \times P_{k_1 l_1}(r_1) P_{k_2 l_2}(r_2) P^{LS}_{l_1 l_2}(r_1, r_2, T), \quad (10)$$

where the box-normalized radial distorted waves P_{kl} are solutions of the one-electron radial Schrödinger equation [5]. The final time solutions $P^{LS}_{l_1 l_2}(r_1, r_2, T)$ are obtained by propagating the Schrödinger equation for the correlated two-electron radial wave function with the total orbital momentum L and spin S to sufficiently long times $t = T$.

TDCS may then be calculated from these amplitudes using the expression [13]

$$\frac{d^3\sigma}{dE_2 d\Omega_1 d\Omega_2} = 2\frac{1}{k_1 k_2}\frac{\omega}{I}\frac{\partial}{\partial t}\int_0^\infty dk_1 \int_0^\infty dk_2\, \delta\left[\beta - \tan^{-1}\left(\frac{k_2}{k_1}\right)\right] \times \sum_{S=0,1} w_S \left| \sum_{l_1, l_2} (-i)^{l_1+l_2} e^{i(\sigma_{l_1}+\sigma_{l_2})} \times P^{LS}_{l_1 l_2}(k_1, k_2, t)\, \boldsymbol{e} \cdot \mathcal{Y}^{l_1 l_2}_L(\boldsymbol{n}_1, \boldsymbol{n}_2) \right|^2, \quad (11)$$

where β is the hyperspherical angle between k_1 and k_2, I is the radiation field intensity and integration over all solid angles, and ejected energy gives the total integral cross section. This expression includes the appropriate spin statistical factors [5] w_S, where $w_0 = 1/4$ and $w_1 = 3/4$. The factor of 2 results from the initial occupation number of the $1s$ orbital.

In the TDCC calculations presented here a (r_1, r_2) radial lattice with $(960)^2$ points with a uniform mesh spacing of $\Delta r = 0.10$ a.u. was used. To fully converge the triple differential cross-section calculations, 9 terms were used for the initial $^{1,3}S$ states and 18 coupled channels were used for the final $^{1,3}P$ states.

The TDCC calculation also uses MPI parallelization to efficiently distribute the calculation over available processors of a parallel machine [14]. The time taken for such calculations depends on the mesh spacing, number of mesh points, and number of angular momenta included in the calculation. The calculations reported here took a few hours on a Linux cluster using 64 processors.

C. Symmetrized DPI amplitudes

The angular momentum summation in the partial wave expansions (8) or (11) can be reduced to the sum over a single angular momentum variable. In the following, we will work out this reduction with the CCC expression (8),

$$\frac{d^3\sigma}{d\Omega_1 d\Omega_2\, dE_2} = C \sum_{S=0,1} \left| \sum_{l=0}^\infty \mathcal{Y}^{ll+1}_{1M}(\boldsymbol{n}_1, \boldsymbol{n}_2) F_{Sll+1}(k_1, k_2) + \mathcal{Y}^{l+1l}_{1M}(\boldsymbol{n}_1, \boldsymbol{n}_2) F_{Sl+1l}(k_1, k_2) \right|^2. \quad (12)$$

We introduce the symmetric and antisymmetric combinations of the matrix elements,

$$F^{\pm}_{Sl_1 l_2}(k_1, k_2) = \tfrac{1}{2}\left\{F_{Sl_1 l_2}(k_1, k_2) \pm (-1)^S\, F_{Sl_2 l_1}(k_1, k_2)\right\}. \quad (13)$$

The bipolar harmonics (9) satisfy the following exchange symmetry relation:

$$\mathcal{Y}^{l_1 l_2}_1(\boldsymbol{n}_1, \boldsymbol{n}_2) = \mathcal{Y}^{l_2 l_1}_1(\boldsymbol{n}_2, \boldsymbol{n}_1). \quad (14)$$

By using Eqs. (13) and (14), the sum in Eq. (12) can be further reduced to

$$\frac{d^3\sigma}{d\Omega_1 d\Omega_2\, dE_2} = C \sum_{S=0,1} \left| \sum_{l=0}^\infty F^+_{Sll+1}(k_1, k_2)\left[\boldsymbol{e} \cdot \mathcal{Y}^{ll+1}_1(\boldsymbol{n}_1, \boldsymbol{n}_2) + (-1)^S \boldsymbol{e} \cdot \mathcal{Y}^{ll+1}_1(\boldsymbol{n}_2, \boldsymbol{n}_1)\right] + F^-_{Sll+1}(k_1, k_2) \times \left[\boldsymbol{e} \cdot \mathcal{Y}^{ll+1}_1(\boldsymbol{n}_1, \boldsymbol{n}_2) - (-1)^S \times \boldsymbol{e} \cdot \mathcal{Y}^{ll+1}_1(\boldsymbol{n}_2, \boldsymbol{n}_1)\right] \right|^2. \quad (15)$$

Then we employ the following expression for the bipolar spherical harmonic [15]:

$$\mathcal{Y}^{ll+1}_1(\boldsymbol{n}_1, \boldsymbol{n}_2) = \frac{(-1)^l}{4\pi}\left(\frac{3}{l+1}\right)^{1/2}\{\boldsymbol{n}_2 P'_{l+1}(x) - \boldsymbol{n}_1 P'_l(x)\}, \quad (16)$$

where $x = \cos\theta_{12} = \boldsymbol{n}_1 \cdot \boldsymbol{n}_2$. This immediately takes us to the final expression for the TDCS,

$$\frac{d^3\sigma}{d\Omega_1 d\Omega_2\, dE_2} = \sum_{S=0,1} \left|(\boldsymbol{e} \cdot \boldsymbol{n}_1 + \boldsymbol{e} \cdot \boldsymbol{n}_2)\, \mathcal{M}^g_S(k_1, k_2, \theta_{12}) + (\boldsymbol{e} \cdot \boldsymbol{n}_1 - \boldsymbol{e} \cdot \boldsymbol{n}_2)\, \mathcal{M}^u_S(k_1, k_2, \theta_{12})\right|^2, \quad (17)$$

where the symmetric *gerade* (g) and antisymmetric *ungerade* (u) DPI amplitudes are

$$\mathcal{M}^{g/u}_S(k_1, k_2, \theta_{12}) = \frac{\sqrt{3C}}{4\pi}\sum_{l=0}^\infty \frac{(-1)^l}{\sqrt{l+1}}[P'_{l+1}(x) \mp (-1)^S P'_l(x)] F^{\pm}_{Sll+1}(k_1, k_2). \quad (18)$$

Owing to the symmetry properties of the matrix elements (6) and definition (13), the amplitudes satisfy the following exchange relations:

$$\mathcal{M}^g_S(k_1, k_2, \theta_{12}) = \mathcal{M}^g_S(k_2, k_1, \theta_{12}), \quad \mathcal{M}^u_S(k_1, k_2, \theta_{12}) = -\mathcal{M}^u_S(k_2, k_1, \theta_{12}). \quad (19)$$

Equation (17) can be simplified further in the special case of the equal energy sharing. In this case $\mathcal{M}^u_S(k_1 = k_2, \theta_{12}) = 0$ and therefore

$$\frac{d^3\sigma}{d\Omega_1 d\Omega_2\, dE_2} = \left|(\boldsymbol{e}\cdot\boldsymbol{n}_1 + \boldsymbol{e}\cdot\boldsymbol{n}_2)\,\mathcal{M}^g_{S=0}(k_1 = k_2, \theta_{12})\right|^2 + \left|(\boldsymbol{e}\cdot\boldsymbol{n}_1 - \boldsymbol{e}\cdot\boldsymbol{n}_2)\,\mathcal{M}^g_{S=1}(k_1 = k_2, \theta_{12})\right|^2 . \quad (20)$$

Thus a pair of symmetric amplitudes is needed to describe the angular distribution of photoelectrons in DPI of Li at equal energy sharing. This is in contrast to DPI of He where the equal energy case requires only one fully symmetric *gerade* amplitude [16]. Similarly, description of DPI of Li without explicit account for the spin would also require just one fully symmetric amplitude for the equal energy sharing case [15].

III. RESULTS

A. Fully resolved TDCS

In Fig. 1 we present the fully resolved TDCS of Li at the excess energy of 10 eV shared equally between the photoelectrons $E_1 = E_2 = 5$ eV. The coplanar geometry is chosen in which the photoelectrons escape in the polarization plane $\phi_1 = \phi_2 = 0$ and the vector $\boldsymbol{e}$ of the 100% linearly polarized light is directed along the z axis (horizontal direction in the figure). In this case $\boldsymbol{e}\cdot\boldsymbol{n}_i = \cos\theta_i$. The escape angle of one of the photoelectrons is fixed to $\theta_1 = 0^\circ$, 30°, 60°, and 90° while the angle of the second photoelectron θ_2 varies over the full 360° range.

The CCC calculation is performed in the velocity gauge as the length gauge is somewhat less reliable due to a limited accuracy of the multiconfiguration ground state. Gauge convergence issues are discussed in our previous publication [6].

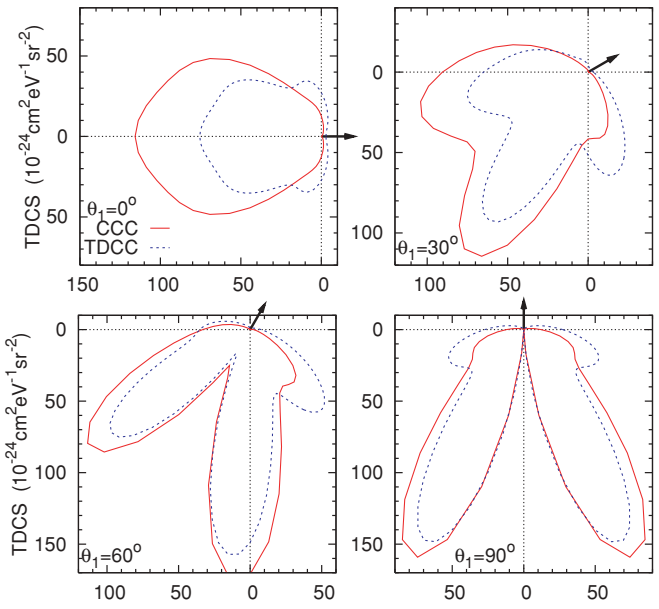

FIG. 1. (Color online) TDCS of DPI of Li at $E_1 = E_2 = 5$ eV and various fixed escape angles $\theta_1 = 0^\circ$, 30°, 60°, and 90° (indicated by the arrow). The CCC calculation is shown by the red solid line whereas the TDCS calculation is displayed with the blue dotted line.

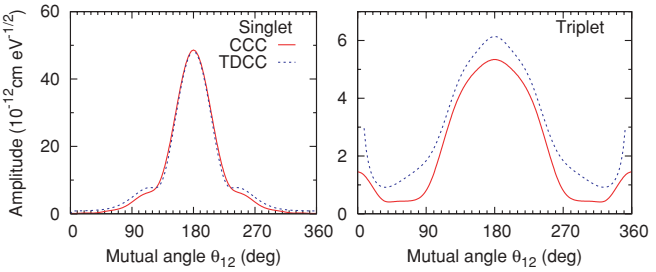

FIG. 2. (Color online) The moduli of the symmetrized DPI amplitudes of Li in the singlet $|\mathcal{M}^g_{S=0}|$ (left) and triplet $|\mathcal{M}^g_{S=1}|$ (right) channels at the equal energy sharings of $E_1 = E_2 = 5$ eV. The CCC amplitudes are shown with red solid lines whereas the TDCC amplitudes are drawn with blue dotted lines.

The TDCC calculation is fully gauge convergent. Even though some differences can be seen between the two calculations, qualitative predictions of the two theories are similar. At smaller fixed angles $\theta_1 = 0^\circ$ and 30° relative to the polarization axis, the two photoelectrons escape predominantly back to back, whereas at larger angles $\theta_1 = 60^\circ$ and 90°, a kinematic node develops at the back-to-back emission and two alternative maxima of the TDCS are formed at the relative photoelectron angles θ_{12} close to 150° and 210°.

This evolution of the TDCS can be conveniently analyzed using Eq. (20). The moduli of the symmetric amplitudes $|\mathcal{M}^g_{S=0}|$ and $|\mathcal{M}^g_{S=1}|$ are plotted on the left and right panels of Fig. 2, respectively. Relative phases of the amplitudes are irrelevant to our analysis as the amplitudes are summed incoherently in Eq. (20). The CCC amplitudes are calculated directly using Eq. (18). In the TDCC formalism, the DPI amplitudes are not evaluated explicitly. Instead, we found them by fitting the TDCS of Fig. 1 with Eq. (20). As is seen from Fig. 2, the singlet amplitude in both models is much larger than its triplet counterpart $|\mathcal{M}^g_{S=0}| \gg |\mathcal{M}^g_{S=1}|$ except for the "tails" of the triplet amplitude near parallel emission $\theta_{12} \simeq 0$. We believe that these tails are unphysical numerical artifacts originating from the Legendre polynomial derivatives $P_l'(x)$ in Eq. (18), which grow rapidly with l at $x \simeq 1$. This growth has to be offset by the rapid fall of the dipole matrix elements $F^{\pm}_{Sll+1}$, which is much harder to achieve for a smaller triplet amplitude. Fortunately, these "tails" have no effect on the TDCS since the triplet amplitude in Eq. (20) is accompanied by the kinematic factor $\cos\theta_1 - \cos\theta_2$, which has a node at the parallel emission $\theta_1 = \theta_2$.

As is seen from Fig. 2, both the CCC and TDCC calculations produce very similar singlet amplitudes but the triplet amplitudes are somewhat different in the two methods. This explains quite a noticeable difference of the CCC and TDCC cross sections at small fixed ejection angles (top two panels of Fig. 1) where the contribution of the triplet amplitude is dominant.

The contribution of the singlet and triplet terms in Eq. (20) is quite different. At small fixed electron angles $\theta_1 \simeq 0$, the mutual angle $\theta_{12} \simeq \theta_2$ and the TDCS becomes

$$\frac{d^3\sigma(\theta_1 = 0)}{d\Omega_1 d\Omega_2\, dE_2} = \left|(1 + \cos\theta_2)\mathcal{M}^g_{S=0}(\theta_2)\right|^2 + \left|(1 - \cos\theta_2)\mathcal{M}^g_{S=1}(\theta_2)\right|^2 . \quad (21)$$

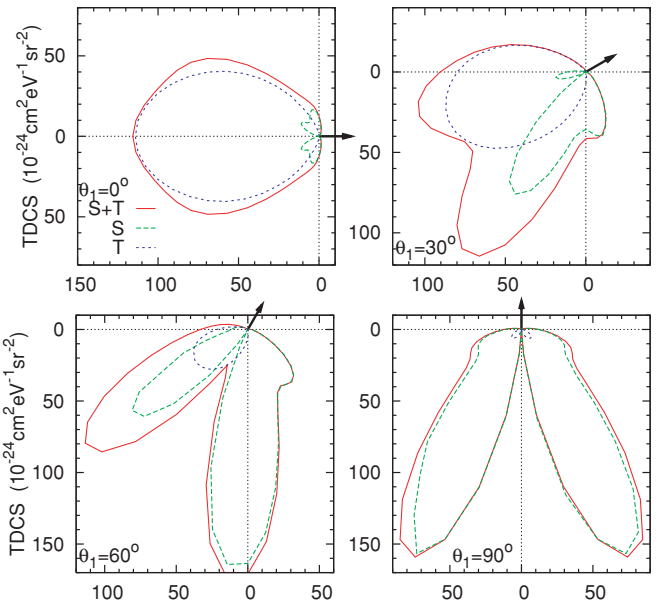

FIG. 3. (Color online) TDCS of DPI of Li at $E_1 = E_2 = 5\,\text{eV}$ and various fixed escape angles $\theta_1 = 0^\circ, 30^\circ, 60^\circ$, and 90° (indicated by the arrow). The CCC calculation is plotted with the sum of the singlet and triplet channels (S+T, red solid line), the singlet channel only (S, green dashed line), and triplet channel only (T, blue dotted line).

We see that the kinematic factor accompanying the singlet amplitude is vanishing at $\theta_2 = \pi$ where $|\mathcal{M}^g_{S=0}(\theta_2)|$ has its maximum whereas the kinematic and the dynamic (amplitude) factors are in concert for the triplet term. Thus, despite being smaller, the triplet amplitude makes the dominant contribution to the TDCS at small fixed ejection angles.

The partial contributions of the singlet (S) and triplet (T) terms are plotted separately in Fig. 3 along with the whole of TDCS, which is the sum of the two terms. Here we plot only CCC results because the TDCC results are very similar. We see that the TDCS at $\theta_1 = 0$ is almost entirely produced by the triplet term contribution. As the fixed ejection angle θ_1 grows, the singlet contribution becomes larger until its contribution becomes strongly dominant at $\theta_1 = 90^\circ$. Indeed, at this angle

$$\frac{d^3\sigma(\theta_1 = 90^\circ)}{d\Omega_1 d\Omega_2\, dE_2} = \Big(\left|\mathcal{M}^g_{S=0}(\theta_2 - 90^\circ)\right|^2 + \left|\mathcal{M}^g_{S=1}(\theta_2 - 90^\circ)\right|^2 \Big) \cos^2\theta_2 \quad (22)$$

and a far bigger singlet amplitude takes over completely.

We see that the interplay of the amplitudes and their associated kinematic factors makes relative contribution of the singlet and triplet channels strongly dependent on the kinematics of the two-electron escape. This is in contrast to the total integrated cross section in which the singlet spin state of the two-electron pair makes the dominant contribution. Wehlitz *et al.* [8] reached this conclusion by drawing an analogy to the metastable He $1s2s$ atom for which the singlet ^1S state has a DPI probability three times higher than the ^3S state [17]. In the TDCS of Li, this analogy to metastable He is completely lost as the pattern of the two-electron escape varies between the one typical for the $1s2s\ ^1S$ state and another characteristic to the $1s2s\ ^3S$ state [18].

We can also see that the lobes of the TDCS become progressively narrower as the fixed ejected angle θ_1 grows. This happens because the singlet amplitude has a much smaller angular spread around its peak at $\theta_{12} = 180^\circ$ in comparison with the triplet amplitude, which is clearly seen in Fig. 2. This spread characterizes the strength of the angular correlation of the two photoelectrons in the singlet and triplet channels. The smaller spread indicates stronger angular correlation, which dictates the photoelectrons to escape in the back-to-back direction to minimize their Coulomb repulsion. Obviously, the strength of the angular correlation is much larger in the singlet channel as compared to the triplet channel. One may think of this in terms of the spatial exchange symmetry of the two-electron continuous wave function. In the singlet channel, this function favors a close encounter of the two photoelectrons $r_1 = r_2$ and it is their angular correlation that keeps them apart. In the meantime, in the triplet channel, the two-electron wave function has a node at $r_1 = r_2$ and the angular correlation may be more liberal as the photoelectrons are kept apart by the force of radial correlation as well.

A somewhat similar disparity in angular correlation width was observed in the quadrupole channel of two-photon DPI of He [19]. This channel exhibits two distinctly different modes of correlated motion of the photoelectron pair. The kinematics of the mode associated with the center-of-mass motion favors large total momenta maximized at parallel emission where the interelectron repulsion is strong. In contrast, the mode associated with the relative motion favors large relative momenta maximized at antiparallel emission where the interelectron repulsion is relatively weak.

IV. CONCLUSION

In the present paper, we perform CCC and TDCC calculations of the fully resolved triply differential cross section of DPI of Li. Both numerical methods have been tested in obtaining the total integrated cross sections of the same process for which they produced very similar results across a wide range of photon energies [20,21]. In comparison to TICS, TDCS is much more sensitive to any approximations made in a calculation, and it is also the most difficult quantity for which to obtain numerical convergence. Thus, it presents a very stringent test to the theory.

Despite some noticeable differences, we regard the level of agreement between the two present calculations as satisfactory, considering the completely independent approaches taken to treat the DPI process. For example, the CCC approach is time-independent and treats the two photoelectrons on a different footing, but it includes the full Hartree-Fock exchange with the nonionized electron. The TDCC approach is time-dependent; it treats both ionized electrons equally but treats the interaction with the nonionized electron through direct and local exchange terms. It is expected that all of these approximations are valid for the process considered here, but it is not so surprising that they could result in small differences in the TDCS for specific energy sharings and geometries. We also note that in comparisons of the equivalent electron-impact process [22], namely the electron-impact ionization of helium,

good agreement is also found between the TDCC and CCC approaches, although the agreement is still not exact.

In addition to numerical calculations, we perform some analytical studies of the TDCS. We show that, under the equal energy sharing condition, the TDCS in lithium can be conveniently parametrized by a pair of symmetrized DPI amplitudes in the singlet and triplet channels. The partial contribution of these amplitudes varies with the fixed escape angle relative to the polarization axis of light. The angular spread of the amplitudes relative to the back-to-back emission indicates the strength of the angular correlation in the two-electron continuum. This strength depends noticeably on the spin of the photoelectron pair.

The observed spin effects are strong in comparison with the weak spin polarization effects which are due to spin-orbit interaction in DPI of heavier atoms [23]. One way to experimentally distinguish the singlet and triplet two-electron continuum states would be to prepare a spin-polarized initial state of the Li atom, which can be achieved by high-field state selection in a sextupole magnet [24]. Then the spin polarization of the Li^{2+} ion should be analyzed after the DPI process. The spin projection flip would unmistakably indicate the triplet spin state of the photoelectron pair. Recently developed mini-Mott spin analyzers [25,26] can also make it possible to determine the photoelectron spin projections directly.

The present report is aimed to provoke further discussion of the mechanisms and pathways of DPI of Li as well as to stimulate more experimental studies of energy- or momentum-resolved differential cross sections. Some of the data resolved with respect to the sum momentum of the photoelectron pair are already reported in the literature [27].

ACKNOWLEDGMENTS

The Los Alamos National Laboratory is operated by Los Alamos National Security, LLC, for the National Nuclear Security Administration of the US Department of Energy under Contract No. DE-AC5206NA25396. A portion of this work was performed through DOE and NSF grants to Auburn University. The computational work was carried out at the National Institute for Computational Sciences in Oak Ridge, TN. Resources of the Australian National Computational Infrastructure (NCI) Facility and its Westeran Australian node iVEC are gratefully acknowledged.

[1] M. T. Huang, R. Wehlitz, Y. Azuma, L. Pibida, I. A. Sellin, J. W. Cooper, M. Koide, H. Ishijima, and T. Nagata, Phys. Rev. A **59**, 3397 (1999).
[2] R. Wehlitz, M. M. Martinez, J. B. Bluett, D. Lujic, and S. B. Whitfield, Phys. Rev. A **69**, 062709 (2004).
[3] J. Colgan, M. S. Pindzola, and F. Robicheaux, Phys. Rev. Lett. **93**, 053201 (2004).
[4] R. Wehlitz, J. Colgan, M. Martinez, J. Bluett, D. Lukic, and S. Whitfield, J. Electron Spectrosc. Relat. Phenom. **144**, 59 (2005).
[5] J. Colgan, D. C. Griffin, C. P. Ballance, and M. S. Pindzola, Phys. Rev. A **80**, 063414 (2009).
[6] A. S. Kheifets, D. V. Fursa, and I. Bray, Phys. Rev. A **80**, 063413 (2009).
[7] G. Mehlman, J. W. Cooper, and E. B. Saloman, Phys. Rev. A **25**, 2113 (1982).
[8] R. Wehlitz, J. B. Bluett, and S. B. Whitfield, Phys. Rev. A **66**, 012701 (2002).
[9] Y. Ralchenko, A. Kramida, J. Reader, and NIST ASD Team, *NIST Atomic Spectra Database*, 3rd ed. (National Institute of Standards and Technology, Gaithersburg, MD, 2008), http://physics.nist.gov/asd3.
[10] A. T. Stelbovics, I. Bray, D. V. Fursa, and K. Bartschat, Phys. Rev. A **71**, 052716 (2005).
[11] D. A. Varshalovich, A. N. Moskalev, and V. K. Khersonskii, *Quantum Theory of Angular Momentum* (World Scientific, Philadelphia, 1988).
[12] D. V. Fursa and I. Bray, Phys. Rev. A **52**, 1279 (1995).
[13] J. Colgan, M. S. Pindzola, and F. Robicheaux, J. Phys. B **34**, L457 (2001).
[14] M. S. Pindzola *et al.*, J. Phys. B **40**, R39 (2007).
[15] N. L. Manakov, S. I. Marmo, and A. V. Meremianin, J. Phys. B **29**, 2711 (1996).
[16] A. S. Kheifets and I. Bray, Phys. Rev. A **65**, 022708 (2002).
[17] A. S. Kheifets, A. Ipatov, M. Arifin, and I. Bray, Phys. Rev. A **62**, 052724 (2000).
[18] J. Colgan and M. S. Pindzola, Phys. Rev. A **67**, 012711 (2003).
[19] A. S. Kheifets, A. I. Ivanov, and I. Bray, Phys. Rev. A **75**, 024702 (2007).
[20] A. S. Kheifets, D. V. Fursa, and I. Bray, Phys. Rev. A **80**, 063413 (2009).
[21] J. Colgan, D. C. Griffin, C. P. Ballance, and M. S. Pindzola, Phys. Rev. A **80**, 063414 (2009).
[22] J. Colgan, M. Foster, M. S. Pindzola, I. Bray, A. T. Stelbovics, and D. V. Fursa, J. Phys. B **42**, 145002 (2009).
[23] N. Chandra, Phys. Rev. A **56**, 1879 (1997).
[24] G. Baum, M. Moede, W. Raith, and W. Schroder, J. Phys. B **18**, 531 (1985).
[25] G. Mankey, S. Morton, J. Tobin, S. Yu, and G. Waddill, Nucl. Instrum. Methods Phys. Res. A **582**, 165 (2007).
[26] R. Berezov, J. Jacoby, T. Rienecker, and J. Schunk, Nucl. Instrum. Methods Phys. Res. A **606**, 120 (2009).
[27] G. Zhu, M. Schuricke, J. Steinmann, J. Albrecht, J. Ullrich, I. Ben Itzhak, T. J. M. Zouros, J. Colgan, M. S. Pindzola, and A. Dorn, Phys. Rev. Lett. **103**, 103008 (2009).